

In vitro testing of a protease-sensitive contrast agent for optoacoustic imaging

Anthony H. Green

James R. Norris

The University of Chicago
Department of Chemistry
5735 S. Ellis Avenue
Chicago, Illinois 60637

Jing Wang

Zhixing Xie

Hao F. Zhang

University of Wisconsin-Milwaukee
Department of Electrical Engineering and Computer
Science
2200 E. Kenwood Boulevard
Milwaukee, Wisconsin 53201-0413

Patrick J. La Riviere

The University of Chicago
Department of Radiology
5841 S. Maryland Avenue
Chicago, Illinois 60637

Abstract. We have designed a protease-sensitive imaging probe for optoacoustic imaging whose absorption spectrum changes upon cleavage by a protease of interest. The probe comprises an active site, a derivative of chlorophyll or natural photosynthetic bacteriochlorophyll that absorbs in the near infrared, conjugated to a peptide backbone specific to the protease being imaged. The uncleaved molecules tend to aggregate in dimers and trimers, causing a change in the absorption spectrum relative to that of the monomer. Upon cleavage, the probe molecules deaggregate, giving rise to a spectrum characteristic of monomers. We show using photospectrometry that the two forms of the probe have markedly different absorption spectra, which could allow for *in vivo* optoacoustic identification using a multiwavelength imaging strategy. Optoacoustic measurements using a narrow-band dye laser find spectral peaks in the two forms of the probe at the expected location. The optoacoustic signal from the uncleaved probe is found to be considerably weaker than that of the cleaved probe, perhaps due to poor optical-acoustic coupling in the aggregated molecules. However, ultimately, it is detection of the cleaved probe that is of the greatest import, since it reports on the protease activity of interest. © 2010 Society of Photo-Optical Instrumentation Engineers. [DOI: 10.1117/1.3365935]

Keywords: photoacoustics; tomography; image reconstruction.

Paper 09362SSPRR received Aug. 18, 2009; revised manuscript received Dec. 23, 2009; accepted for publication Dec. 28, 2009; published online Mar. 29, 2010.

1 Introduction

We are working to develop a molecular imaging agent that will allow for *in vivo* imaging of proteases by use of optoacoustic tomography (OAT). Proteases are protein-cleaving proteins known to be overactive in a number of pathologies, including cancers and vascular disease. Elevated levels of proteases such as cathepsins and matrix metalloproteinases (MMPs) are associated with a number of tumor types, and these proteolytic enzymes participate in tissue invasion, metastasis, and angiogenesis processes.¹⁻⁵ The ability to detect abnormal proteolytic activity levels could allow for detection of cancers well before they manifest themselves anatomically. This would also allow for molecular profiling of tumors, which would facilitate treatment planning and would allow for monitoring of the molecular response to treatment.⁶

While the strategy we are developing can in principle be employed for any protease by incorporating the appropriate peptide sequence into the probe, we have chosen to focus on MMP-2 (gelatinase 72KDa) in this study. MMPs are extracellular proteases involved in the degradation of the extracellular matrix (ECM); MMP-2 is secreted both by tumor cells and by stromal cells in an inactive form that is activated through proteolytic cleavage by membrane-type MMPs (MT-MMPs).⁷

MMPs are overexpressed in many tumor types, and expression levels appear to correlate with tumor stage and metastasis.⁸ In addition to simply detecting MMP-2 levels, the ability to image MMP-2 activity would allow for monitoring of the response to MMP-2 inhibitor therapy.⁹

1.1 Optical Approaches to Protease Imaging

The most widely pursued strategy for *in vivo* protease imaging has involved pure optical imaging of activatable probes containing near-infrared (NIR) fluorophores. This approach has been pioneered by the group of Ralph Weissleder at Massachusetts General Hospital and has been recently commercialized for small animal imaging by VisEn Medical. The molecular probes typically comprise pairs of mutually quenching fluorophores or a fluorophore and a dedicated quencher that are linked to each other or to a backbone molecule by peptide spacers that are cleavage targets for the protease of interest.^{6,10-16} In the uncleaved state, the molecule is relatively quiescent due to the fluorescence quenching, but upon cleavage by the target protease, the fluorescence activity increases several fold. The simplest such construct involves simply attaching fluorophores to either end of an appropriate protease-substrate peptide chain.¹⁷

A longer-circulating probe was obtained by use of a larger molecule featuring a polyethylene glycol protected graft co-

Address all correspondence to: Patrick J. La Riviere, The University of Chicago, Department of Radiology, 5841 S. Maryland Avenue, MC-2026, Chicago, IL 60637. Tel: 773-702-6975; Fax: 773-702-3766; E-mail: pjlariviere@uchicago.edu

polymer (PGC), comprising a poly-L-lysine backbone to which are attached methoxy polyethylene glycol (MPEG) side chains.¹⁸ Other side chains held mutually quenching, near-infrared fluorophores or combinations of fluorophores and dedicated quenchers.^{14,19} The fluorophores are generally chosen to absorb and emit in the near-infrared (700 to 1100 nm) range to maximize tissue penetration.

Once cleaved, these activatable probes can be imaged by a number of different optical approaches, including simple fluorescent reflectance imaging or fluorescent endoscopic imaging,^{20,21} which involve stimulating fluorescence by illuminating the sample at appropriate wavelengths and then detecting the emitted fluorescence photons on the same side of the subject using appropriate filters. These approaches are simple and cost effective but provide neither fully three-dimensional (3-D) nor quantitative information.

Quantitative three-dimensional information can be obtained by a more sophisticated fluorescence molecular tomography (FMT) approach.^{13,22,23} In FMT, near-infrared light is directed into the subject from a number of different directions, and the resulting fluorescent photons as well as the scattered incident photons are detected outside the subject. The problem of reconstructing the distribution of fluorophores from this set of measurements is similar in principle to that in diffuse optical tomography, and it allows for formation of quantitative three-dimensional images, albeit with limited depth penetration, resolution, and sensitivity, as discussed in the following.

Optical techniques such as FMT have been used primarily in small-animal imaging and have practical limitations that may restrict their widespread application in human imaging. Due to the strong optical scattering of the both excitation and fluorescent light in biological tissues, the resulting images have resolution limited to the millimeter range. The best reported resolution is approximately 1 mm in a fairly optimized planar geometry with the fluorophore at a depth of 0.75 cm, centered between two imaging plates separated by 1.5 cm (Ref. 24). The resolution would be expected to worsen for a more deeply seated structure. In addition, the strong scattering and absorption of the fluorescent photons limits the sensitivity of FMT, which in the same planar imaging device just discussed, was shown to have a detection threshold of 100 fmol of fluorophore (Cy 5.5) at a depth of 0.75 cm (Ref. 24). Again, this sensitivity would fall off at greater depths, although overall sensitivity could conceivably be improved by advances in photon-detection technology.²⁴

1.2 Potential Advantages of Optoacoustic Protease Imaging

Optoacoustic imaging can potentially overcome many of the limitations of the pure optical imaging approach. While OAT can, of course, be used to measure innate optical absorption properties of the body, it can also be used to detect strongly absorbing molecular probes that are introduced into the body.²⁵⁻²⁷ Kruger et al. have shown that the basic fluorescing imaging agents employed in FMT also produce a detectable optoacoustic signal.²⁵⁻²⁷ In fact, because the fluorescence yield of many agents is relatively low (for Cy5.5, it is 0.28), more of the absorbed optical energy goes into producing heat, and thus into producing an optoacoustic signal, than goes into fluorescence. Kruger et al. demonstrated that their OAT sys-

tem can detect as little as 5 fmol of fluorophore (Cy 5.5) at 1.25 cm depth in a tissue mimicking phantom, which is over an order of magnitude better sensitivity than has been reported for FMT.²⁵⁻²⁷

More recently, Razansky et al. have shown that optoacoustic techniques can be used to image green fluorescent proteins at greater depth and sensitivity than pure optical detection techniques.²⁸

Wang's group has demonstrated the use of such agents *in vivo*, performing optoacoustic imaging of live mice after injection of indocyanine green (ICG), which absorbs strongly in the near-infrared. They were able to detect as little as 7 pmol of ICG per resolution element against the strong absorption background of blood.²⁹ They have recently performed *in vivo* imaging of gene expression using the b-Gal/X-Gal system, whereby b-Gal is used as a reporter gene behind a promoter of interest and X-Gal as a cleavable substrate. When cleaved by b-Gal, X-Gal, which is originally colorless, produces a blue product that absorbs strongly in the near-infrared and can be imaged by OAT.³⁰

Naturally, the quenched fluorophore strategy employed in FMT for protease imaging cannot be applied directly in OAT, which is sensitive to the absorption rather than the fluorescence properties of the contrast agents. This is the motivation for the absorption-shifting cleavable probe that we are developing.³⁵

2 Design and Synthesis of the Molecular Probe

2.1 Overview of Probe Design

We have designed a molecular probe for *in vivo* optoacoustic imaging of local protease activity. The molecule is designed so that its optical absorption properties are altered when it is cleaved by a protease of interest. Specifically, the probe comprises an active site, a derivative of chlorophyll or natural photosynthetic bacteriochlorophyll that absorbs in the near infrared, conjugated to a peptide backbone specific to the protease being imaged. The uncleaved molecules tend to aggregate in dimers and trimers, causing a change in the absorption spectrum relative to that of the monomer. Upon cleavage, the probe molecules tend to deaggregate, giving rise to a spectrum characteristic of monomers.

2.2 Background on Chlorophyll and Bacteriochlorophyll

The chlorophylls are a family of porphyrin-derived chromophores naturally found in the photosynthetic system of plants and photosynthetic bacteria.³¹ The most common form found in plants is chlorophyll *a* (Chl *a*), while bacteriochlorophyll *a* (Bchl *a*) is the most common in bacteria. Both compounds are strongly absorbent pigments with molar extinction coefficients over 10,000 M⁻¹ cm⁻¹. As with other porphyrins, there are four electronic transitions, creating four absorption bands, with the lowest in energy being at approximately 680 nm for Chl *a* and approximately 780 nm for Bchl *a* (Ref. 31).

In order to use Chl *a* or Bchl *a* in an imaging probe, a coupling point, which is not present in their native forms, must be created. The ester linking the phytol chain to the main ring is easily hydrolyzed to form a coupling point in either compound. While it is possible to remove the phytol chain

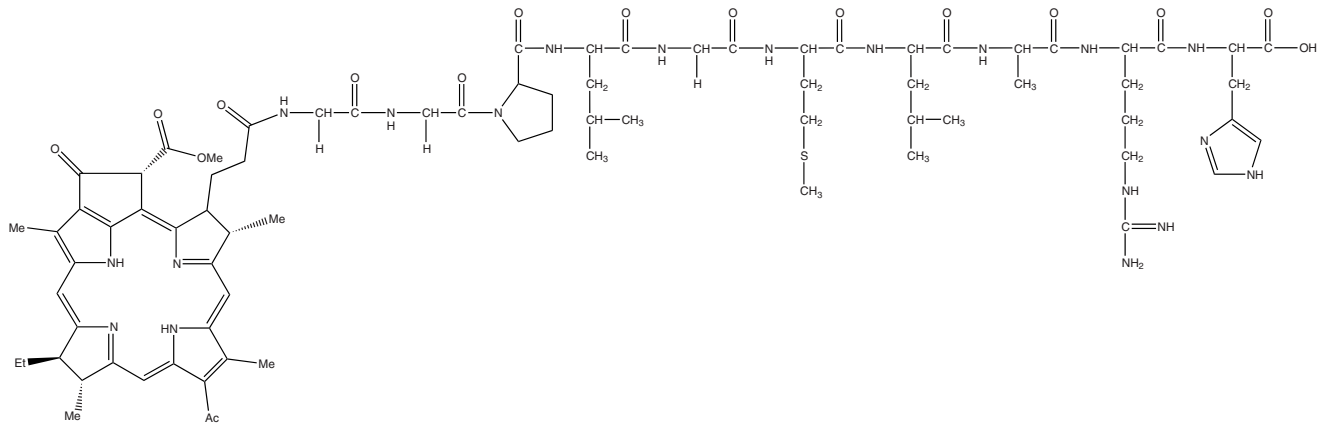


Fig. 1 Probe design using the sequence HO-HRALMGLPGG-Phe.

without affecting any other portion of the structure, it is cleaner to hydrolyze the ester with trifluoroacetic acid (TFA) and remove the central magnesium in the same step.³¹ This converts Chl *a* to pheophorbide *a* (Phe *a*) and Bchl *a* to bacteriopheophorbide *a* (Bphe *a*). The consequence of using Phe *a* or Bphe *a* is a blue shift of 20 nm in the absorption spectra relative to that in natural compound.

An absorption-shifting phenomenon can occur in any of the four aforementioned compounds upon aggregation. In this phenomenon, a shift in the optical absorption spectrum is observed when two or more of the chromophores are in close proximity. The extent of the optical shift is determined by the distance of separation and the relative orientations of the macrocycles.³² The chlorophylls, including Bchl *a*, are particularly known for aggregating into dimers or oligomers under the right conditions, resulting in optical absorption spectra exhibiting large red shifts of the lowest electronic transition.³³ Increasing numbers of molecules aggregating does somewhat increase the red shift relative to that of the dimer, but with diminishing returns: the increase in absorption shift decays exponentially as more molecules are added to the aggregate, so most of the shift is explained by the difference between the monomer and dimer forms. This means that when oligomers are formed, large differences in the number of components have very little effect on the absorption spectrum. Lewis acid-base and π - π interactions play significant roles in determining the structure of the aggregate.³³ The Lewis acid-base interaction occurs when the ketone group donates electron density to an empty orbital of the center magnesium. The π - π interaction occurs when the flat rings stack on top of each other, allowing overlap between the π orbitals. Typical optical spectra of monomer and dimer forms of Bchl *a* will be shown in the following, indicating a 40-nm shift. Depending on the system, as much as a 70-nm shift has been observed for the red-most band of the optical spectrum of Bchl *a* dimers and oligomers.³⁴

Similarly, the reaction center of the photosynthetic complex contains two chlorophyll *a* molecules in close contact to each other and exhibits an absorption peak at 700 nm. Upon isolation of chlorophyll from the plant material, the absorption peak shifts to 662 nm. This change is due to a phenomenon associated with the aggregation of chromophores. When

two or more chromophores—in this case, chlorophyll *a*—are in close proximity, the electric field around each chromophore will change the energy associated with the absorption spectrum.

It is these aggregation-based shifts that we exploit in the design of the protease-sensitive optoacoustic probe.

2.3 Details of the Probe Design

As depicted in Fig. 1, the probe comprises simply a peptide chain with a Phe or Bphe attached at the N-terminus. The working design targets MMP-2 with the peptide sequence HRALMGLPG, where each letter stands for a specific amino acid. The protease cleaves the peptide between the methionine (M) and the glycine (G) residues. Prior to cleavage, the probe aggregates in semisoluble micelles. After the addition of MMP-2, the micelles are broken apart, and the cleaved portions become monomers. This is illustrated schematically in Fig. 2.

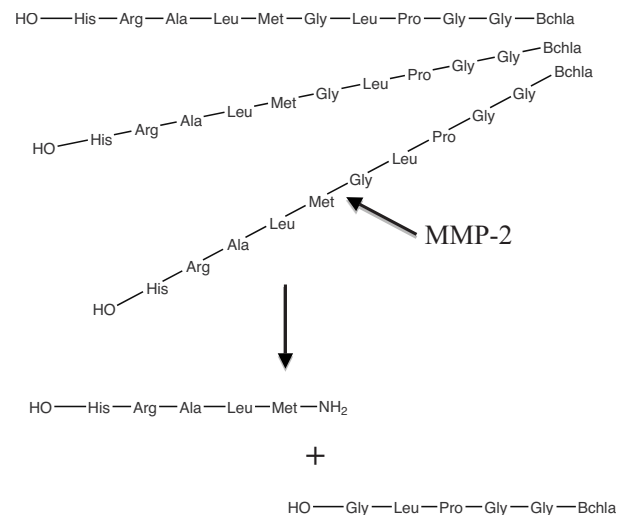


Fig. 2 Schematic of the probe behavior. Prior to cleavage, the probe molecules tend to aggregate, bringing the Chl or Bchl into dimers, trimers, and higher-order aggregates. After cleavage, the cleaved moieties tend to float free, producing monomer Chl or Bchl.

3 Experimental Methods

3.1 Solvent-Induced Aggregation of Bacteriochlorophyll *a*

We conducted a preliminary study to explore the absorption spectra that we could expect from the monomer and dimer forms of Bchl *a*, since the difference between these two spectra is what will allow us to detect cleaving of our probe molecule by proteases, which results in the conversion of Bchl and Chl dimers and trimers to monomers. By carefully controlling the solvent conditions, aggregation of pure Bchl *a* can be created or destroyed.

3.1.1 Method

Bchl *a*, isolated by standard means³¹ from the photosynthetic bacterium *Rhodobacter sphaeroides* routinely grown in our laboratory, is dried via vacuum distillation in anhydrous petroleum ether. This drying process removes most although not all of the water coordinated to Bchl *a*, such that approximately a 3:2 molar ratio of Bchl *a*:H₂O still existed. The dried Bchl *a* is dissolved in carbon tetrachloride. Dimers are formed by the ketone of one Bchl *a* serving as the fifth ligand to the Mg of another Bchl *a*. Adding a drop of pyridine disrupts this interaction, causing the mixture to become purely monomeric. The resulting solution is placed in an optical cell, and the absorption spectrum was recorded using a Shimadzu UV-1602 UV-visible spectrophotometer.

3.2 Synthesis of the Probe

The probe was synthesized with standard solid-phase peptide synthesis techniques.³⁶ A custom synthesized fluorine labile resin was used as the solid support.³⁷ The peptide was then built sequentially from the c-terminus and capped with Phe *a*. The sequence was cleaved from the resin, washed, and then evaporated to dryness. The resulting peptide was dissolved in the enzyme reaction buffer described in Sec. 3.3.

3.3 Enzymatic Cleavage of the Imaging Probe

The cleavage procedure³⁸ follows the protocol provided by the enzyme producer, NovaBioChem. A solution of 5 mM NaCl, 5 mM CaCl₂, and 0.01 M ethylenediaminetetraacetic acid (EDTA) in water is prepared. Two milliliters of the solution is added to approximately 200 mg of the dry, solvent-free imaging probe and stirred at 30 °C until fully dissolved. The 5 units of the MMP-2 enzyme at room temperature are added to the probe solution. The solution was stirred and complete cleavage generally took less than 15 min.

3.4 Optical Spectroscopy

We used optical light spectroscopy to measure the molar extinction coefficient as a function of wavelength for the uncleaved and cleaved forms of the sample. A Shimadzu UV-1602 UV-visible spectrophotometer was coupled to a desktop PC and used for the acquisition of all extinction coefficient spectra. The purity of Bchl *a*/Chl *a* and carotenoid mixtures can be determined with optical spectroscopy along with the state of aggregation. Furthermore, the high extinction coefficient of Bchl *a* ($\epsilon=42.0 \times 10^3$ in methanol³¹) and Chl *a* ($\epsilon=70.5 \times 10^3$ in methanol³¹) allows for good absorption with extremely low concentrations.

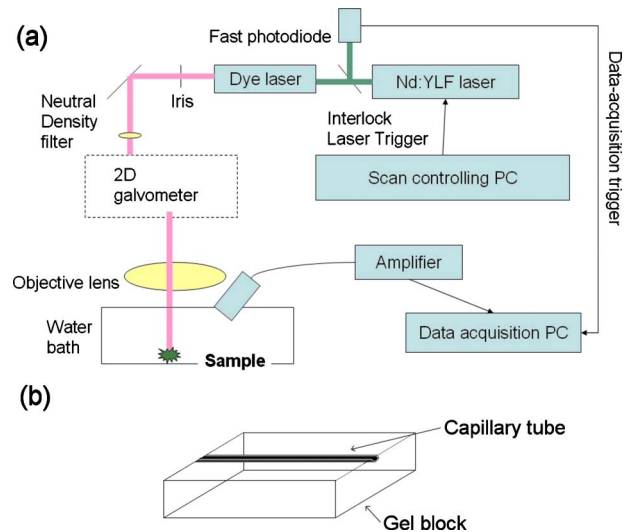


Fig. 3 (a) Schematic of the optoacoustic microscopy system. (b) Schematic of the sample.

After the synthesis of the probe, the sample was dissolved in methylene chloride and divided into two equal (by volume) aliquots. The methylene chloride was completely removed by vacuum evaporation, and the solid probe was dissolved in 2 ml of enzyme buffer solution. The absorption spectra were taken consecutively using either a 1-cm, 5-mm, or 1-mm path length cuvette, depending on the concentration of the sample. Generally, the uncleaved samples required the usage of the 1-mm or 5-mm cuvette, while the cleaved sample performed well in the 5-mm and 1-cm cuvettes. The absorbance A of each sample was calculated as

$$A = -\log(I/I_0),$$

where I is the transmitted intensity through the sample, and I_0 the intensity of the illuminating beam. The molar extinction coefficient ϵ can then be calculated as $\epsilon=A/cl$, where c is the molar concentration of the absorber, and l is the cuvette thickness.

3.5 Optoacoustic Microscopy

Optoacoustic measurements were performed using the microscopic system described in Xie et al.³⁹ and illustrated in Fig. 3(a). In this system, the illumination is focused to a diffraction-limited spot to provide the lateral resolution, and an unfocused transducer provides the depth resolution by mapping the measured temporal signals into the image volume in a B-scan mode. The illumination point can be scanned rapidly using a standard galvanometer scanner.

The samples were the same as those used to obtain the optical extinction coefficient spectra, except they were transferred to a different imaging cell. A 0.5-mm inside diameter, 0.7-mm outside diameter Teflon tube was placed at the surface of a plastic weighting boat full of hot gelatin gel (gelatin from bovine skin, Sigma-Aldrich, St. Louis, Missouri). The gel was allowed to cool, trapping the tube at the surface of the gel, as shown schematically in Fig 3(b). Ultrasound gel (Clear

Image, Sonotech, Bellingham, Washington) was spread over the top of the agar gel to facilitate ultrasonic coupling, and all visible air bubbles were carefully removed.

The sample was illuminated by laser pulses (pulse repetition rate: 1 kHz; pulse duration: 6 ns) from a tunable dye laser (Cobra, Sirah Laser and Plasmatechnik GmbH, Germany) pumped by an Nd:YLF laser (IS811-e, EdgeWave GmbH, Germany). The beam output from the dye laser, which is not spatially homogeneous, was spatially filtered by an iris and expanded to an 8-mm diameter. The beam then passed sequentially through a neutral density filter and a 60-mm focal length objective lens. The beam then passed into an imaging basin filled with water (depth: 30 mm). The pulse energy was around 0.1 μJ , and the energy density at the optical focus was around 200 mJ/cm^2 . This energy density was higher than the ANSI maximum permissible exposure (MPE) for wavelengths shorter than 700 nm (20 mJ/cm^2) but did not exceed the MPE for wavelengths longer than 700 nm (200 mJ/cm^2).

A single-element, unfocused transducer (V313, Olympus NDT; 15 MHz; bandwidth: 80%; active element diameter: 6 mm) was submerged in the water at an angle of 15 deg to the incidental laser beam at the sample. The recorded optoacoustic signals were amplified by 58 dB and were digitized and stored by high-speed digitizer (CS12400, Gage Applied, Lockport, Illinois) for further processing. At each optical wavelength, the optoacoustic signal was recorded 512 times, allowing for the calculation of a mean and standard deviation.

3.5.1 Laser properties

The optoacoustic experiment was performed in two parts with two different laser dyes because no single laser dye available would scan over the entire desired range of wavelengths. Part 1 used the dye LDS 722 (nominal tuning range is 691 to 751 nm when pumped at 532 nm; Exciton, Inc.) and covered the wavelengths around the cleaved probe peak (655 to 690 nm) while part 2 used the dye oxazine 720 (nominal tuning range is 613 to 708 nm when pumped at 532 nm; Exciton, Inc.) and covered the uncleaved probe peak (695 to 740 nm).

There is pulse-by-pulse energy variation that could be compensated for by recording the laser pulse energy for each PA measurement. In this study, however, we averaged the signal 512 times. The pulse energy instability should be minimized through signal averaging, as the laser system has an energy instability of less than 5% (root-mean-square value). We used the water signal as an internal calibration standard, correcting all the signals in a wavelength-dependent fashion such that the spectral properties of water agreed with their known values from the literature. The imaging system is being upgraded in a manner that should allow for true spectroscopic measurements in the future with careful monitoring of the wavelength-dependent output of the laser.

4 Results

4.1 Optical Properties of Bacteriochlorophyll

The spectra resulting from the experiment described in Sec. 3.1 are shown in Fig. 4, where it can be seen that the monomer form of Bchl *a* has an absorption peak at 782 nm, while

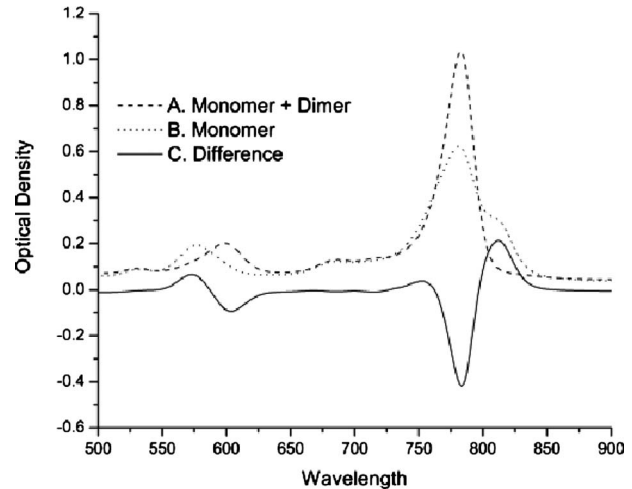


Fig. 4 Optical absorption spectra of bacteriochlorophyll *a* monomer and dimer. A: Bchl *a* in semidry carbon tetrachloride. Water coordinated to central Mg prevents aggregation, resulting in blue-shifted monomers. Dimers of Bchl *a* form when water is not coordinated to Mg, resulting in the red-shifted shoulder at about 820 nm. B: Same as solution A but with addition of 100-fold excess (relative to Bchl *a*) of pyridine that strongly coordinates with Mg, preventing any aggregation, resulting in a single transition peak centered at 782-nm. C: Difference spectrum between solutions A and B, clearly showing the optical shift accompanying Bchl *a* dimerization.

the dimer absorption peak is shifted to approximately 820 nm.

4.2 Ultraviolet-Visible Light Spectroscopy of Complete Probe

The extinction coefficient spectra for the tubes containing the probe with and without cleavage by MMP-2 are shown in Fig. 5. In its whole state, the probe produces aggregates (dimers and trimers) that give rise to a broad absorption spectrum with a peak at 726 nm. After addition of MMP-2, the probe is cleaved, and the aggregates are not reformed. The sharp peak in the spectra at 668 nm is characteristic of a monomer, as the energy levels are distinct, whereas an aggregate will have a

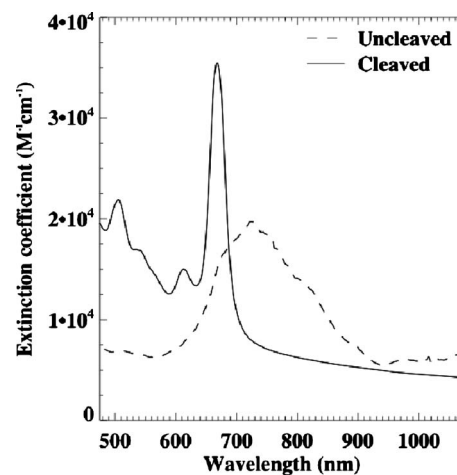


Fig. 5 Extinction coefficient spectra of the probe without (uncleaved) and with (cleaved) the addition of MMP-2.

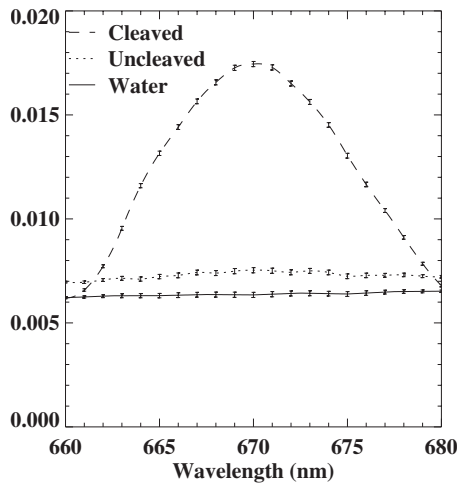


Fig. 6 Measurements made in the range 660 to 680 nm on tubes containing the probe before and after cleavage with MMP-2, as well as a tube containing water alone.

broad absorption peak due to the various possible dipole angles between the Chl or Bchl in the aggregates. The absorption of an individual aggregate creates a peak of the same bandwidth as the monomer, although shifted to be centered at a different wavelength. As the angle, θ , between the two dipoles changes, the magnitude of the red shift in absorption increases or decreases. The superposition of all these shifted absorption peaks creates the broad overall absorption peak seen. The concentration of the samples was $\sim 140 \mu\text{M}$, so the monomer peak corresponds to an extinction coefficient of approximately $35,000 \text{ M}^{-1} \text{ cm}^{-1}$.

4.3 Optoacoustic Results

The measured, calibrated peak-to-peak optoacoustic signals obtained with each laser are plotted. The results obtained with the Oxazine 720 laser, which should cover the peak of the cleaved probe, are shown in Fig. 6. As expected from the extinction coefficient spectra, the cleaved probe has a very strong peak centered near 666 nm. The uncleaved probe absorbs much less strongly than the cleaved probe in this range, as expected. In this range, the uncleaved probe signal is consistently twice as strong as that of the water in the control tube, however.

The results obtained with the LDS 722 laser, which should cover the peak of the uncleaved probe, are shown in Fig. 7. The uncalibrated results, in which the differences among the curves are more clearly visible, are shown in Fig. 8. The uncleaved probe produces a clear peak near 730, as expected from the extinction coefficient spectrum, although it is somewhat weaker than expected. The cleaved probe also appears to be absorbing much more strongly relative to the uncleaved probe than would have been expected from the extinction coefficient spectrum.

There are several potential explanations for the relatively weak signal from the uncleaved form of the probe, although these are all necessarily speculative and will require further experimentation to resolve. One explanation is that the uncleaved probe has a smaller Grüneisen parameter than expected. The Grüneisen parameter (Γ) is the efficiency of the

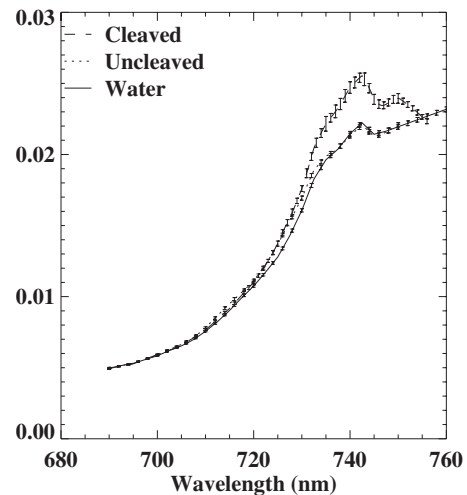


Fig. 7 Measurements made in the range 695 to 755 nm on tubes containing the probe before and after cleavage with MMP-2, as well as a tube containing water alone.

conversion of absorbed light energy into acoustic energy. The interaction between the aggregates could be interfering with the thermal expansion by reducing the expansion of the absorber when irradiated. A second potential explanation would be the presence of transient absorption changes due to alternative pathways for the deactivation of the excited aggregates, a phenomenon that has actually been observed in porphyrin aggregates, which are chemically similar to the molecules we are employing.⁴⁰

5 Discussion and Conclusions

We have designed a protease-sensitive imaging probe for optoacoustic tomography whose absorption spectrum changes upon cleavage by a protease of interest. The probe comprises an active site, a derivative of chlorophyll or natural photosynthetic bacteriochlorophyll that absorbs in the near infrared, conjugated to a peptide backbone specific to the protease be-

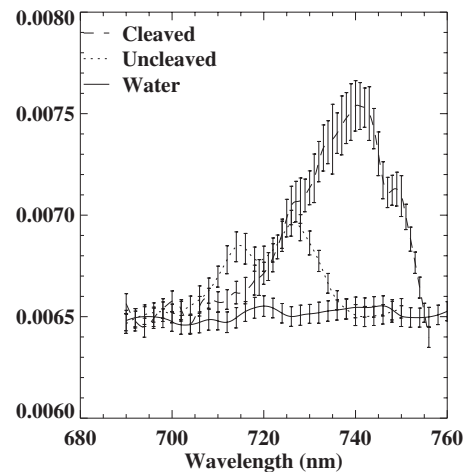


Fig. 8 Raw, uncalibrated measurements made in the range 695 to 755 nm on tubes containing the probe before and after cleavage with MMP-2, as well as a tube containing water alone.

ing imaged. The uncleaved molecules tend to aggregate in dimers and trimers, causing a change in the absorption spectrum relative to that of the monomer. Upon cleavage, the probe molecules tend to deaggregate, giving rise to a spectrum characteristic of monomers.

The absorption spectra of the cleaved and uncleaved probes as measured by the spectrophotometer differed significantly. It should thus be possible to distinguish the two forms of the probe during imaging by use of a multiwavelength chromophore identification strategy. While the cleaved probe signal is clearly of greatest interest, since it reports on protease activity, it would be helpful to be able to image both states. This would allow for more robust quantitation of protease activity, based on the ratio of cleaved to uncleaved probe detected. However, the optoacoustic results suggested that the uncleaved form of the probe produced a weaker-than-expected optoacoustic signal, perhaps due to poorer coupling of optical into acoustic energy in the chlorophyll aggregates. This might make it challenging to detect the uncleaved form of the probe at depth *in vivo*. Nonetheless, it is ultimately the cleaved form of the probe that is of greatest interest.

A limitation of all cleavable, activatable molecular probes for protease detection (including the fluorescent probes described in Sec. 1.1) is a lack of perfect substrate specificity. Proteases other than the target protease will invariably also cleave the substrate, although typically to a much lesser extent. The consequences of this lack of specificity will depend to some extent on the purpose of the protease imaging. Since it appears that protease imaging would be used mainly to judge the aggressiveness of the cancer in invading the ECM and monitoring response to protease inhibitors (which are themselves not perfectly specific), some cross-cleavage by other ECM proteases would not compromise the utility of the images.

The version of the probe tested here was based on chlorophyll rather than bacteriochlorophyll. Chlorophyll was easier to work with in proof-of-concept experiments since it can be extracted from spinach, among other plants. Versions based on bacteriochlorophyll are expected to behave essentially identically, with the principal difference being that both the cleaved and uncleaved spectral peaks would much farther in the near-infrared, which could be beneficial for deep tissue imaging.

In future work, we plan to study the sensitivity of the probe to various concentrations of MMP-2 *in vitro* as well to study its specificity to cleavage by MMP-2 as opposed to other MMPs and members of different protease families such as cathepsins. We will seek to establish the safety of the probe by performing toxicology and biokinetic studies in a mouse model. Last, we will seek to perform optoacoustic imaging in a mouse model with two xenograft tumors, one from a cell line known to overexpress MMP-2 and one known not to overexpress MMP-2.

Acknowledgments

This work was supported in part by American Cancer Society Research Scholar Grant RSG-08-117-01-CCE to Patrick La Riviere and in part by the University of Wisconsin-Milwaukee startup fund and a grant from The Lynde and Harry Bradley Foundation to Hao F. Zhang. Anthony Green is a principal in AVAS Partners, a consulting and technology development

firm that may seek to further develop and commercialize the molecular imaging agent reported in this manuscript if they succeed in licensing the technology from the University of Chicago. Patrick La Riviere has no current affiliation with AVAS but would receive royalties if the company licensed the technology from the University of Chicago and would potentially join the board of scientific advisers.

References

1. D. Keppler, M. Sameni, K. Moin, T. Mikkelsen, C. Diglio, and B. Sloane, "Tumor progression and angiogenesis: cathepsin B & Co.," *Biochem. Cell Biol.* **74**, 799–810 (1996).
2. M. Garcia, N. Platlet, E. Liaudet, V. Laurent, D. Derocq, J. P. Brouillet, and H. Rochefort, "Biological and clinical significance of cathepsin D in breast cancer metastasis," *Stem Cells* **14**, 642–650 (1996).
3. M. J. Davies, "Reactive oxygen species, metalloproteinases, and plaque stability," *Circulation* **97**, 2383–2383 (1998).
4. H. Rochefort, M. Garcia, M. Glondu, V. Laurent, E. Liaudet, J. M. Rey, and P. Roger, "Cathepsin D in breast cancer: mechanisms and clinical applications, a 1999 overview," *Clin. Chim. Acta* **291**, 157–170 (2000).
5. I. Podgorski and B. Sloane, "Cathepsin B and its role(s) in cancer progression," *Biochem. Soc. Symp.* **70**, 263–276 (2000).
6. U. Mahmood and R. Weissleder, "Near-infrared optical imaging of proteases in cancer," *Molecular Cancer Ther.* **2**(5), 489–496 (2003).
7. M. Egeblad and Z. Werb, "New functions for the matrix metalloproteinases in cancer progression," *Nat. Rev. Cancer* **2**, 163–176 (2002).
8. I. Stamenkovic, "Matrix metalloproteinases in tumor invasion and metastasis," *Semin Cancer Biol.* **10**(6), 415–433 (2000).
9. C. Bremer, C.-H. Tung, and R. Weissleder, "In vivo molecular target assessment of metalloproteinase inhibition," *Nat. Med.* **7**, 743–748 (2001).
10. A. Wunder, C.-H. Tung, U. Muller-Ladner, R. Weissleder, and U. Mahmood, "In vivo imaging of protease activity in arthritis: a novel approach for monitoring treatment response," *Arthritis Rheum.* **50**, 2459–2465 (2004).
11. C. Bremer, C.-H. Tung, A. J. Bogdanov, and R. Weissleder, "Imaging of differential protease expression in breast cancers for detection of aggressive tumor phenotypes," *Radiology* **222**, 814–818 (2002).
12. R. Weissleder, C.-H. Tung, U. Mahmood, and A. Bogdanov, Jr., "In vivo imaging of tumors with protease activated near-infrared fluorescent probes," *Nat. Biotechnol.* **17**, 375–378 (1999).
13. V. Ntziachristos, C.-H. Tung, C. Bremer, and R. Weissleder, "Fluorescence molecular tomography resolves protease activity *in vivo*," *Nat. Med.* **8**(7), 757–760 (2002).
14. M. Funovics, R. Weissleder, and C.-H. Tung, "Protease sensors for bioimaging," *Anal. Bioanal. Chem.* **377**(6), 956–963 (2003).
15. M. F. Kircher, R. Weissleder, and L. Josephson, "A dual fluorochrome probe for imaging proteases," *Bioconjugate Chem.* **15**, 242–248 (2004).
16. W. Pham, R. Weissleder, and C.-H. Tung, "Developing a peptide-based near-infrared molecular probe for protease sensing," *Bioconjugate Chem.* **15**, 1403–1407 (2004).
17. W. Pham, R. Weissleder, and C.-H. Tung, "An azulene dimer as a near-infrared quencher," *Angew. Chem.* **41**(19), 3659–3662 (2002).
18. A. J. Bogdanov, C. Martin, A. Bognanova, T. Brady, and R. Weissleder, "An adduct of cis-diamminedichloroplatinum(II) and poly(ethylene glycol)poly(L-lysine)-succinate: synthesis and cytotoxic properties," *Bioconjugate Chem.* **7**(1), 144–149 (1996).
19. C.-H. Tung, S. Bredow, U. Mahmood, and R. Weissleder, "Preparation of a cathepsin D sensitive near-infrared fluorescence probe for imaging," *Bioconjugate Chem.* **10**, 892–896 (1999).
20. U. Mahmood, C.-H. Tung, Y. Tang, and R. Weissleder, "Feasibility of *in vivo* multichannel optical imaging of gene expression: experimental study in mice," *Radiology* **224**, 446–451 (2002).
21. C. Bremer, S. Bredow, U. Mahmood, R. Weissleder, and C.-H. Tung, "Optical imaging of matrix metalloproteinase-2 activity in tumors: feasibility study in a mouse model," *Radiology* **221**(2), 523–529 (2001).
22. V. Ntziachristos, C. Bremer, E. Graves, J. Ripoll, and R. Weissleder, "In vivo tomographic imaging of near-infrared fluorescent probes," *Mol. Imaging* **1**, 82–88 (2002).
23. J. Chen, C.-H. Tung, U. Mahmood, V. Ntziachristos, R. Gyrko, M.

- Fishman, P. Huang, and R. Weissleder, "In vivo imaging of proteolytic activity in atherosclerosis," *Circulation* **105**(23), 2766–2771 (2002).
24. E. Graves, J. Ripoll, R. Weissleder, and V. Ntziachristos, "A submillimeter resolution fluorescence molecular imaging system for small animal imaging," *Med. Phys.* **30**(5), 901–911 (2003).
 25. R. A. Kruger, W. L. Kiser, G. A. Kruger, and K. D. Miller, "Thermoacoustic optical molecular imaging of small animals," *Mol. Imaging* **2**, 113–123 (2003).
 26. M. C. Pilatou, E. Marani, F. F. M. de Mul, and W. Steenbergen, "Photoacoustic imaging of brain perfusion on albino rats by using Evans blue as contrast agent," *Arch. Physiol. Biochem.* **111**, 389–397 (2003).
 27. G. Ku and L. Wang, "Deeply penetrating photoacoustic tomography in biological tissues enhanced with an optical contrast agent," *Opt. Lett.* **30**, 507–509 (2005).
 28. D. Razansky, M. Distel, C. Vinegoni, R. Ma, N. Perrimon, R. W. Koster, and V. Ntziachristos, "Multispectral opto-acoustic tomography of deep-seated fluorescent proteins *in vivo*," *Nature Photon.* **3**, 412–417 (2009).
 29. X. Wang, G. Ku, M. Wegiel, D. Bornhop, G. Stoica, and L. Wang, "Noninvasive photoacoustic angiography of animal brains *in vivo* with near-infrared light and an optical contrast agent," *Opt. Lett.* **29**(7), 730–732 (2004).
 30. R. J. Zemp, L. Li, S. Fimilache, G. Lungu, G. Stoica, and L. Wang, "Imaging of gene expression *in vivo* with photoacoustic tomography," *Proc. SPIE* **6086**, 608608 (2006).
 31. H. Scheer, Ed. *Chlorophylls*, CRC Press, Boca Raton, FL (2000).
 32. E. G. McRae and M. Kasha, "Enhancement of phosphorescence ability upon aggregation of dye molecules," *J. Chem. Phys.* **28**(4), 721–722 (1958).
 33. K. Ballschmitter and J. J. Katz, "An infrared study of chlorophyll-chlorophyll and chlorophyll-water interactions," *J. Am. Chem. Soc.* **91**(10), 2661–2676 (1969).
 34. A. Scherz and V. Rosenbach-Belkin, "Comparative study of optical absorption and circular dichroism of bacterchlorophyll oligomers in Triton X-100, the antenna pigment B850 and the primary donor P-860 of photosynthetic bacteria indicated that all are similar dimers of bacteriochlorophyll a," *Proc. Natl. Acad. Sci. U.S.A.* **86**, 1505–1509 (1989).
 35. P. La Riviere, A. Green, and J. R. Norris, "Development of a protease-sensitive molecular imaging agent for optoacoustic tomography," *Proc. SPIE* **6437**, 64370K (2007).
 36. M. Schnolzer, P. F. Alewood, A. Jones, D. Alewood, and S. Kent, "In situ neutralization in Boc-chemistry solid-phase peptide synthesis," *Int. J. Pept. Protein Res.* **40**, 180–193 (1992).
 37. A. Routledge, H. T. Stock, S. L. Flitsch, and N. J. Turner, "New fluoride-labile linkers for solid-phase organic synthesis," *Tetrahedron Lett.* **38**(47), 8287–8290 (1997).
 38. T. Xia, K. Akers, A. Z. Eisen, and J. L. Sltzer, "Comparison of cleavage site specificity of gelatinases A and B using collagenous peptides," *Biochim. Biophys. Acta* **1293**, 259–266 (1996).
 39. Z. Xie, S. Jiao, H. F. Zhang, and C. A. Puliafito, "Laser-scanning optical-resolution photoacoustic microscopy," *Opt. Lett.* **34**(12), 1771–1773 (2009).
 40. R. F. Khairutdinov and N. Serpone, "Laser-induced light attenuation in solutions of porphyrin aggregates," *J. Phys. Chem.* **99**, 11952–11958 (1995).